clean technologies

MDPI

Article

Coupling a Gas Turbine Bottoming Cycle Using CO_2 as the Working Fluid with a Gas Cycle: Exergy Analysis Considering Combustion Chamber Steam Injection

S. Hamed Fatemi Alavi [1], Amirreza Javaherian [1], S. M. S. Mahmoudi [1], Saeed Soltani [1,*] and Marc A. Rosen [2]

[1] Faculty of Mechanical Engineering, University of Tabriz, Tabriz 16471, Iran; hamed.f.alavi98@ms.tabrizu.ac.ir (S.H.F.A.); a_javaherian@tabrizu.ac.ir (A.J.); s_mahmoudi@tabrizu.ac.ir (S.M.S.M.)
[2] Faculty of Engineering and Applied Science, University of Ontario Institute of Technology, 2000 Simcoe Street North, Oshawa, ON L1G 0C5, Canada; marc.rosen@ontariotechu.ca
* Correspondence: saeed929@tabrizu.ac.ir; Tel.: +98-9144-067-078

Abstract: Gas turbine power plants have important roles in the global power generation market. This paper, for the first time, thermodynamically examines the impact of steam injection for a combined cycle, including a gas turbine cycle with a two-stage turbine and carbon dioxide recompression. The combined cycle is compared with the simple case without steam injection. Steam injection's impact was observed on important parameters such as energy efficiency, exergy efficiency, and output power. It is revealed that the steam injection reduced exergy destruction in components compared to the simple case. The efficiencies for both cases were obtained. The energy and exergy efficiencies, respectively, were found to be 30.4% and 29.4% for the simple case, and 35.3% and 34.1% for the case with steam injection. Also, incorporating steam injection reduced the emissions of carbon dioxide.

Keywords: combined cycle; gas turbine; steam injection; recompression supercritical carbon dioxide; energy analysis; exergy analysis

check for updates

Citation: Fatemi Alavi, S.H.; Javaherian, A.; Mahmoudi, S.M.S.; Soltani, S.; Rosen, M.A. Coupling a Gas Turbine Bottoming Cycle Using CO_2 as the Working Fluid with a Gas Cycle: Exergy Analysis Considering Combustion Chamber Steam Injection. *Clean Technol.* **2023**, *5*, 1115–1139. https://doi.org/10.3390/cleantechnol5030056

Academic Editor: Leonid Tartakovsky

Received: 5 August 2023
Revised: 12 September 2023
Accepted: 18 September 2023
Published: 21 September 2023

Copyright: © 2023 by the authors. Licensee MDPI, Basel, Switzerland. This article is an open access article distributed under the terms and conditions of the Creative Commons Attribution (CC BY) license (https://creativecommons.org/licenses/by/4.0/).

1. Introduction

Energy and environmental impact analyses have gained importance in recent years due to increasing concerns over hydrocarbon fuel consumption and environmental pollution [1]. Recently, international agreements have attempted to decrease fuel consumption and environmental pollution, as well as retire many fossil fuel power plants [2]. The electricity production market is also changing. Between 2015 and 2035, nearly 90 GW of fossil fuel power plant capacity will be retired in the United States [3]. Meanwhile, natural gas power plants are gradually increasing in number. Gas turbines play a prominent role in electricity generation technology today, with the potential to grow. Nearly 80 GW of new gas turbine power plant capacity is predicted to enter the electricity generation market by 2035 [4].

Decreasing fuel consumption for a given output makes power plants operate more economically by reducing fuel consumption costs. However, a capital cost investment is normally required to obtain high efficiency and is offset by fuel cost savings. Gas turbine cycles can work on an extensive range of fuels comprising natural gas, which exhibits cleaner combustion than other fossil fuels [5–7]. In designing new gas turbine units, it is often advantageous to increase turbine inlet temperatures and pressure ratios. Other beneficial gas turbine modifications include the use of intercoolers and interstage turbine reheat [8–10]. Gas turbines power generation plants can also incorporate solid oxide fuel cells [11–13].

Nowadays, the utilization of gas turbine power plants incorporating steam injection to the combustor with natural gas is one of the most effective ways for the reduction of NOx emissions. Such plants also have relatively good energy efficiencies. Exhaust gases

can be used to produce superheated steam, which is one of the most effective heat recovery methods [14].

A thorough review of wet gas turbine research [15] identified those cycles having the highest future potential. Romeliotis and Mathiodakis [16] analyzed the effect of water injection on engine efficiency and performance as well as on compressor behavior. Techniques were investigated for water injection through internal methods that ascertain water injection influences on the gas turbine and on compressor off-design performance. Enhanced performance for the gas turbine was demonstrated with water injection. Eshati et al. [17] presented a model for industrial gas turbines to investigate the impacts on heat transfer and cooling of turbine blades of the air-water ratio. It was shown that, with a rise in the air-water ratio, the cooling temperature of the blade inlet was reduced along the blade opening. The temperature of blade metal in each part was reduced as the air-water ratio increased, and this also increased the creep life of the blade.

Renzi et al. [18] evaluated the effects of syngas (produced gas) and its performance in a gas microturbine with steam injection (SI). The results showed that the energy of the synthesis gas in the combustion chamber (CC) reduced NOx emissions by nearly 75%. In contrast, the CO emissions increased slightly with natural gas combustion. It was found that the maximum value of injected steam in the combustion chambers of the gas turbine system was 56 g/s. Mazzocco and Rukni [19] thermodynamically investigated a parallel analysis for solid oxide fuel cell plants, hybrid gas turbines with steam injection, gasification power plant combinations, and simple power plants. For the optimized power plants, the energy and exergy efficiencies were shown to be 53% and 43%, respectively, significantly more than the related values for conventional 10 MW power plants fed with biomass. A thermo-economic analysis identified the average cost of electricity for the arrangements with the best performance at EUR 6.4 and 9.4/kW, which is competitive in the marketplace.

Using energy, exergy, economic and environmental analyses, Amiri-Rad [20] investigated steam injection and heat recovery for a gas turbine having steam injection in addition to an anti-surge system. Waste heat recovery via a heat exchanger produced steam from the gas turbine exhaust. Finally, the employed method introduced the optimal steam injection conditions for the combustion chamber; for a relative humidity of 10% and an ambient temperature of 38 °C, the optimal steam temperature was observed to be 318.5 °C. Steam injection to the gas turbine with integrated thermal recovery at the optimal steam temperature reduced the cost of electricity production by 25.5% and increased the net generated power by 56 MW and the energy efficiency by 4.6%.

Ahmed [21] examined a modified gas turbine by injecting steam between the combustion chamber exit and turbine entrance. Current optimized cycles having steam injection yield higher power output and efficiency, which results in lower specific costs. Bahrami et al. [22] improved gas turbine transient performance through steam injection during a frequency drop. A control system was presented that, during the frequency drop, utilized an auxiliary input of steam injection to enhance gas turbine transient performance. The control algorithm's performance was investigated at several conditions, demonstrating that steam injection increased the performance notably for the standard control algorithm, particularly near full load conditions.

Sun et al. [23] performed energy, exergy, and exergoeconomic investigations of two systems using supercritical CO_2 combined with a gas turbine. They considered the effects on energy efficiency of five parameters, including temperature difference of the inlet and outlet for exhaust gases, pressure ratio, and compressor inlet pressure. They also obtained values of the exergy efficiency and cost per kilowatt hour. Comparing the traditional combined cycle and the design proposed, they reported that the S-CO_2 cycle had competitive economic performance without any significant thermodynamic performance loss.

In the present work, a gas turbine cycle using a working fluid of carbon dioxide is examined, with steam injection to the combustion chamber (SIGTSC) and without (GTSC). Then, the cycle variations are compared. The novelty of this work lies mainly in (1) the proposal of a power generation system with two subsystems (gas turbine cycle with

steam injection and two-stage turbine and SCO_2 subsystem) in a combined form, and (2) ascertaining the effects of steam injection percentage to the combustion chamber on the overall system performance with an in-depth analysis (considering ten combustion products) to elicit more realistic results. The steam injection also improves the system's environmental characteristics like carbon dioxide emissions, which are important today.

2. Description of System

Figure 1 depicts the considered system, which consists of a SCO_2 recompression bottoming cycle and a Brayton topping cycle as the cycle. Air enters the air compressor at ambient atmospheric conditions; then air, methane, and superheated steam flows mix at different conditions, and the combustion process occurs. Hot exhaust gases are conveyed to the two-stage gas turbine where work is produced and the temperature decreases. The SCO_2 subsystem utilizes exhaust gases as a high-temperature heat source. The SCO_2 cycle is described elsewhere [24,25]. After transferring heat from the output gases in the HEX heat exchanger, the cooled gases enter the HRSG and supply the superheated steam used by the combustion chamber. In this study, the efficiency was examined for the power generation system with two subsystems (gas turbine cycle with steam injection and two-stage turbine and SCO_2 subsystem) in a combined form, as were the effects on the whole system of steam injection percentage to the combustion chamber.

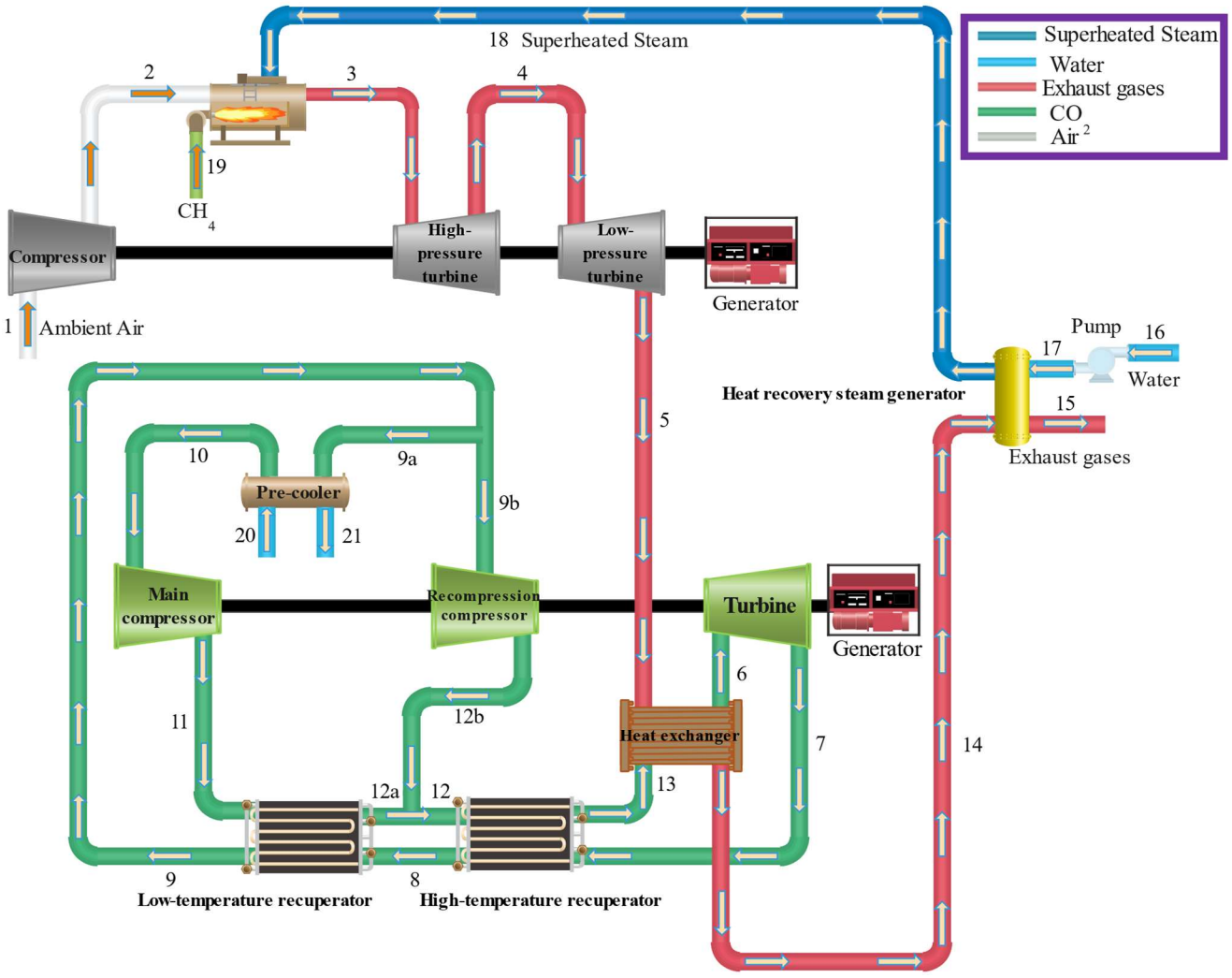

(**a**)

Figure 1. *Cont.*

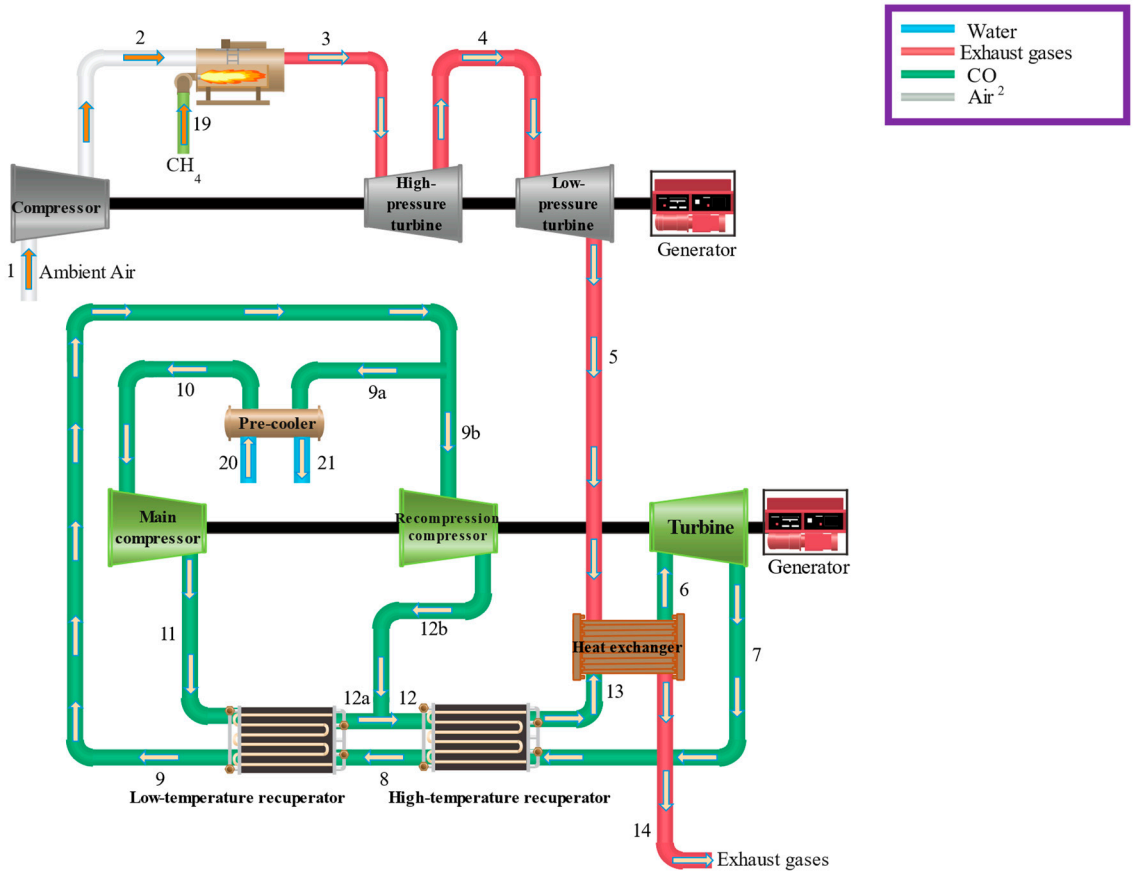

(**b**)

Figure 1. (**a**). Steam injection gas turbine with supercritical carbon dioxide (SIGTSC). (**b**). Gas turbine with supercritical carbon dioxide (GTSC).

Various approximations and simplifications were invoked during the analysis:

- All gases were assumed ideal with specific heat and enthalpy changes depending on the temperature, except for injected steam.
- Nitrogen and oxygen compression factors were assumed to be ideal even at the lowest temperature and highest pressure of the analysis.
- Due to thermodynamic restrictions, the turbine inlet temperature could not exceed 1440 K.
- The air entering the compressor was considered completely dry and contained 21% oxygen and 79% kmol nitrogen on a molar basis.
- The combustion chamber efficiency in the gas turbines utilizing natural gas and methane in gas phases was very high and, in most studies, a value of 99% has been considered.
- Combustion was considered to be steady, and the CC was considered a well-stirred reactor (WSR).
- The temperature of combustion was based slightly on the stoichiometric rich side. This was performedbecause Lefebvre [26] showed that, for a fixed enthalpy of reactants, the lower the product mixture average specific heat is, the higher the resulting flame temperature is because of the richer average specific heat for the products.
- In the Brayton subsystem of recompression of supercritical carbon dioxide, the system operated at steady flow, and variations in kinetic and potential energies could be disregarded [24,25].
- Pressure drops due to friction were negligible [27].

- Pressure losses and heat losses in all heat exchangers and pipelines could be disregarded [24].

3. Modeling and Simulation

3.1. Energy Analysis

The first law of thermodynamics was employed to balance energy rates for the power generation components. Following conservation of mass principles, mass flow rates and molar flow rates of flows of working fluids were determined. For a control volume operating at steady state, general rate balances for mass and energy, respectively, are:

$$\sum \dot{m}_i = \sum \dot{m}_e \tag{1}$$

$$\dot{Q}_{cv} - \dot{W}_{cv} = \Sigma \dot{m}_i h_i - \Sigma \dot{m}_e h_e \tag{2}$$

Here, $\dot{W}_{cv}$ and $\dot{Q}_{cv}$, respectively, denote the power and the heat transfer rate into the control volume.

For the simulation, EES software was used.

3.1.1. Combustion Modeling

Combustion Process with Steam Injection

In the present work, the incoming air from the compressor was mixed in the combustion chamber with fuel (methane), while superheated steam was injected through the process to control the emissions of pollutants to the environment. The chemical reaction occurring in the CC was as follows [28,29]:

$$\varepsilon\varphi CH_4 + (0.21O_2 + 0.79N_2) + xH_2O \rightarrow \nu_1 CO_2 + \nu_2 H_2O + \nu_3 N_2 + \nu_4 O_2 + \nu_5 CO + \nu_6 H_2 + \nu_7 H + \nu_8 O + \nu_9 OH + \nu_{10} NO \tag{3}$$

Here, φ and ε are the equivalence ratio and the molar air-fuel ratio, respectively, while x denotes the injection molar ratio of H_2O. These quantities can be written, respectively, as follows: [28,29].

$$\phi = \frac{(F/A)_{actual}}{(F/A)_{stochiometric}} \tag{4}$$

$$\varepsilon = \frac{0.21}{2} \tag{5}$$

$$x = \frac{MW_{air}}{MW_{H2O}} s \tag{6}$$

In Equation (4), s is the steam injection ratio. Usually, designs of gas turbines allow up to 5% of steam injection into the CC [30]. The molar balance for the 10 species in Equation (1) of the combustion reaction are related as follows:

$$C: \ \varepsilon\phi = \nu_1 + \nu_5 \tag{7}$$

$$H: \ 4\varepsilon\varphi + 2\,x = 2\nu_2 + 2\nu_6 + \nu_7 + \nu_9 \tag{8}$$

$$O: \ 0.42 + x = 2\nu_1 + \nu_2 + 2\nu_4 + \nu_5 + \nu_8 + \nu_9 + \nu_9 + \nu_{10} \tag{9}$$

$$N: \ 1.58 = 2\nu_3 + \nu_{10} \tag{10}$$

Also, there are six chemical balances among the species in of combustion products according to the following [28]:

$$H_2 \rightleftarrows 2H \tag{11}$$

$$O_2 \rightleftarrows 2O \tag{12}$$

$$2H_2O \rightleftarrows 2OH + H_2 \tag{13}$$

$$O_2 + N_2 \rightleftarrows 2NO \tag{14}$$

$$CO_2 + H_2 \rightleftarrows CO + H_2O \tag{15}$$

$$2CO_2 \rightleftarrows 2CO + O_2 \tag{16}$$

The chemical equilibrium constants for the above reactions are obtained according to the following equations [28,29]:

$$K_s = \exp\left(-\frac{\Delta\overline{G}_S}{\overline{R}T_{product}}\right) \tag{17}$$

$$K_1 = \frac{{\nu_7}^2}{\nu_6}\left(\frac{P_3}{P_0 N_{tot}}\right) \tag{18}$$

$$K_2 = \frac{{\nu_8}^2}{\nu_4}\left(\frac{P_3}{P_0 N_{tot}}\right) \tag{19}$$

$$K_3 = \frac{\nu_6 {\nu_9}^2}{{\nu_2}^2}\left(\frac{P_3}{P_0 N_{tot}}\right) \tag{20}$$

$$K_4 = \frac{{\nu_{10}}^2}{\nu_4 \nu_3} \tag{21}$$

$$K_5 = \frac{\nu_5 \nu_2}{\nu_1 \nu_6} \tag{22}$$

$$K_6 = \frac{{\nu_5}^2 \nu_4}{{\nu_1}^2}\left(\frac{P_3}{P_0 N_{tot}}\right) \tag{23}$$

In Equation (17), $T_{product}$ is the temperature of combustion products. Also, $\Delta\overline{G}_S$ denotes the variation in Gibbs function of chemical equilibrium reactions in the atmospheric pressure and is obtained from the following:

$$\Delta\overline{G}_1 = 2\overline{g}_H - \overline{g}_{H_2} \tag{24}$$

$$\Delta\overline{G}_2 = 2\overline{g}_O - \overline{g}_{O_2} \tag{25}$$

$$\Delta\overline{G}_3 = 2\overline{g}_{OH} + \overline{g}_{H_2} - 2\overline{g}_{H_2O} \tag{26}$$

$$\Delta\overline{G}_4 = 2\overline{g}_{NO} - \overline{g}_{O_2} - \overline{g}_{N_2} \tag{27}$$

$$\Delta\overline{G}_5 = 2\overline{g}_{CO} + \overline{g}_{H_2O} - \overline{g}_{CO_2} - \overline{g}_{H_2} \tag{28}$$

$$\Delta\overline{G}_6 = 2\overline{g}_{CO} + \overline{g}_{O_2} - 2\overline{g}_{CO_2} \tag{29}$$

In the above equations, $\overline{g}_i$ is the molar Gibbs function of species i in exhaust gases, and the chemical equilibrium at the atmospheric pressure is obtained using the following [31]:

$$\overline{g}_i = \overline{h}_i\left(\mathrm{T} = \mathrm{T}_{product}\right) - \mathrm{T}_{product}\overline{s}_i\left(\mathrm{T} = \mathrm{T}_{product}, \mathrm{P} = \mathrm{P}_0\right) \quad (30)$$

After determining the chemical equilibrium constant and solving the set of chemical equations of the combustion reaction, the numbers of moles of products in the CC were determined.

Combustion Process without Steam Injection

For the simple conventional gas turbine system without steam injection, the combustion process under complete chemical equilibrium conditions is as follows:

$$CH_4 + 2/\varphi(O_2 + 3.76N_2) \rightarrow \nu_1 CO_2 + \nu_2 H_2O + \nu_3 N_2 + \nu_4 O_2 + \nu_5 CO + \nu_6 H_2 + \nu_7 H + \nu_8 O + \nu_9 OH + \nu_{10} NO \quad (31)$$

The molar balances for the species in the chemical equation are presented in Equations (32)–(35):

$$\mathrm{C}: \ 1 = \nu_1 + \nu_5 \quad (32)$$

$$\mathrm{H}: \ 4 = 2\nu_2 + 2\nu_6 + \nu_7 + \nu_9 \quad (33)$$

$$\mathrm{O}: \ \frac{4}{\varphi} = 2\nu_1 + \nu_2 + 2\nu_4 + \nu_5 + \nu_8 + \nu_9 + \nu_{10} \quad (34)$$

$$\mathrm{N}: \ \frac{15.04}{\varphi} = 2\nu_3 + \nu_{10} \quad (35)$$

The chemical equilibrium equations are exactly the same as the steam injection mode (see Equations (11)–(29)).

3.1.2. Analysis of Expansion

For the high operating pressure associated with the proposed gas turbine system, a two-stage turbine was utilized in the configuration, as shown in Figure 1. The HPT and LPT pressure ratios can be written as [32]:

$$\mathrm{Pr}_{\mathrm{HPT}} = \frac{\mathrm{P}_3}{\mathrm{P}_4} \quad (36)$$

$$\mathrm{Pr}_{\mathrm{LPT}} = \frac{\mathrm{P}_4}{\mathrm{P}_5} \quad (37)$$

where

$$\mathrm{P}_4 = \sqrt{\mathrm{P}_3 \times \mathrm{P}_5} \quad (38)$$

Energy balance equations of the component used in the proposed plant are presented in Table 1

The first law efficiency expressions for each subsystem of the plant in both the steam injection and simple modes are as follows:

$$(\eta_{\mathrm{I}})_{\mathrm{STIG}} = \frac{\dot{\mathrm{W}}_{\mathrm{net}}}{\dot{\mathrm{m}}_{\mathrm{f}} \times \mathrm{LHV}_{\mathrm{CH4}}} \quad (39)$$

$$(\eta_{\mathrm{I}})_{\mathrm{SCO2}} = \frac{\dot{\mathrm{W}}_{\mathrm{net}}}{\dot{\mathrm{Q}}_{\mathrm{HEX}}} \quad (40)$$

$$(\eta_I)_{tot,SIGTSC} = \frac{\dot{W}_{HPT} + \dot{W}_{LPT} - \dot{W}_{comp} - \dot{W}_{pump} + \dot{W}_{Turb} - \dot{W}_{mc} - \dot{W}_{rc}}{\dot{m}_f \times LHV_{CH4}} \quad (41)$$

$$(\eta_I)_{tot,GTSC} = \frac{\dot{W}_{HPT} + \dot{W}_{LPT} - \dot{W}_{comp} + \dot{W}_{Turb} - \dot{W}_{mc} - \dot{W}_{rc}}{\dot{m}_f \times LHV_{CH4}} \quad (42)$$

Table 1. Energy rate balance relations for the components of the power generation system.

Steam injection gas turbine subsystem with two-stage turbine	
Device	Energy rate balance
Air compressor	$\dot{H}_1 + \dot{W}_{comp} = \dot{H}_2$
CC	$\dot{H}_2 + \dot{H}_{18} + \dot{H}_{19} = \dot{H}_3 + \dot{Q}_{los}$
HPT	$\dot{H}_4 + \dot{W}_{HPT} = \dot{H}_3$
LPT	$\dot{H}_5 + \dot{W}_{LPT} = \dot{H}_4$
HRSG	$\dot{H}_{15} + \dot{H}_{18} = \dot{H}_{14} + \dot{H}_{17}$
Pump	$\dot{H}_{16} + \dot{W}_{Pump} = \dot{H}_{17}$
Brayton subsystem with supercritical carbon dioxide working fluid	
Device	Energy rate balance
Main compressor	$\dot{H}_{10} + \dot{W}_{mc} = \dot{H}_{11}$
Recompression compressor	$\dot{H}_{9_b} + \dot{W}_{rc} = \dot{H}_{12_b}$
Turbine	$\dot{H}_6 = \dot{H}_7 + \dot{W}_{Turb}$
LTR	$\dot{H}_{11} + \dot{H}_8 = \dot{H}_{12_a} + \dot{H}_9$
HTR	$\dot{H}_{12} + \dot{H}_7 = \dot{H}_8 + \dot{H}_{13}$
HEX	$\dot{H}_5 + \dot{H}_{13} = \dot{H}_6 + \dot{H}_{14}$
Pre-cooler	$\dot{H}_{9_a} + \dot{H}_{20} = \dot{H}_{10} + \dot{H}_{21}$

3.2. Exergy Analysis

We now write exergy rate balances for the power generation system components and to determine the irreversibility rate of each. For a control volume at steady state, a general exergy rate balance can be written as [33]:

$$\Sigma \dot{E}_i + \Sigma \dot{Q}_j \left(1 - \frac{T_0}{T_j}\right) = \Sigma \dot{E}_e + \dot{W}_{cv} + \dot{I}_{cv} \quad (43)$$

Here, $\Sigma \dot{Q}_j \left(1 - \frac{T_0}{T_j}\right)$ represents the exergy rate with heat transfer, while T_j denotes the temperature where heat is transferred. $\dot{I}_{cv}$ represents the internal irreversibility rate, which is always a positive quantity. The working fluid's total exergy flow rate $\dot{E}$ is the sum of the thermodynamic and chemical flow exergy rates [33]. That is,

$$\dot{E} = \dot{E}_{th} + \dot{E}_{ch} \quad (44)$$

For a working fluid, the exergy flow rate can be written as [33]:

$$\dot{E}_{th} = \Sigma \dot{m}_i [(h_i - h_0) - T_0(s_i - s_0)] \quad (45)$$

where $\dot{m}_i$, h_i, and s_i, respectively, denote the mass flow rate, specific enthalpy, and the specific entropy for the working fluid at state i; and h_0 and s_0, respectively, are the specific

enthalpy and entropy for the working fluid at the dead state. The chemical exergy flow rate for a mixture of ideal gases is expressible as follows [33]:

$$\dot{E}_{ch} = \dot{n}\left(\Sigma\, y_i\, \overline{e}_i^{ch.0}\, \overline{R}T_0 \Sigma\, y_i \ln\left(\, y_i\right)\right) \tag{46}$$

Here, y_i denotes species i molar fraction for the mixture, and $\overline{e}_i^{ch.0}$ standard chemical exergy of an ideal gas. According to Figure 1, exergy rate balance relationships are listed in Table 2 for each power generation system device.

Table 2. Exergy rate balance relations for the components of the power generation system.

Steam injection gas turbine subsystem with two-stage turbine	
Component	Exergy rate balance
Air compressor	$\dot{E}_1 + \dot{W}_{comp} = \dot{E}_2 + \dot{I}_{comp}$
CC	$\dot{E}_2 + \dot{E}_{18} + \dot{E}_{19} = \dot{E}_3 + \dot{I}_{cc} + \dot{Q}_{loss}\left(1 - \frac{T_0}{T_3}\right)$
HPT	$\dot{E}_4 + \dot{W}_{HPT} + \dot{I}_{HPT} = \dot{E}_3$
LPT	$\dot{E}_5 + \dot{W}_{LPT} + \dot{I}_{LPT} = \dot{E}_4$
HRSG	$\dot{E}_{18} + \dot{E}_{15} = \dot{E}_{14} + \dot{E}_{17} + \dot{I}_{HRSG}$
Pump	$\dot{E}_{16} + \dot{W}_{pump} = \dot{E}_{17} + \dot{I}_{pump}$
Brayton subsystem with supercritical carbon dioxide working fluid	
Component	Exergy rate balance
Main compressor	$\dot{E}_{10} + \dot{W}_{mc} = \dot{E}_{11} + \dot{I}_{mc}$
Recompression compressor	$\dot{E}_{9_b} + \dot{W}_{rc} = \dot{E}_{12_b} + \dot{I}_{rc}$
Turbine	$\dot{E}_6 = \dot{E}_7 + \dot{W}_{Turb} + \dot{I}_{Turb}$
LTR	$\dot{E}_{11} + \dot{E}_8 = \dot{E}_{12_a} + \dot{E}_9 + \dot{I}_{LTR}$
HTR	$\dot{E}_{12} + \dot{E}_7 = \dot{E}_8 + \dot{E}_{13} + \dot{I}_{HTR}$
HEX	$\dot{E}_5 + \dot{E}_{13} = \dot{E}_6 + \dot{E}_{14} + \dot{I}_{HEX}$
Pre-cooler	$\dot{E}_{9_a} + \dot{E}_{20} = \dot{E}_{10} + \dot{E}_{21} + \dot{I}_{percooler}$

To examine the quality of energy obtained from the power generation system, the exergy efficiency (sometimes referred to as second law efficiency) was used. For each of the existing subsystems, as well as the overall system, the exergy efficiencies were as follows:

$$(\eta_{II})_{STIG} = \frac{\dot{W}_{net}}{\dot{E}_{19}} \tag{47}$$

$$(\eta_{II})_{SCO2} = \frac{\dot{W}_{net}}{\dot{E}_5 - \dot{E}_{14}} \tag{48}$$

$$(\eta_{II})_{tot,SIGTSC} = \frac{\dot{W}_{HPT} + \dot{W}_{LPT} - \dot{W}_{comp} - \dot{W}_{pump} + \dot{W}_{Turb} - \dot{W}_{mc} - \dot{W}_{rc}}{\dot{m}_f \times \dot{E}_{ch,CH4}} \tag{49}$$

$$(\eta_{II})_{tot,GTSC} = \frac{\dot{W}_{HPT} + \dot{W}_{LPT} - \dot{W}_{comp} + \dot{W}_{Turb} - \dot{W}_{mc} - \dot{W}_{rc}}{\dot{m}_f \times \dot{E}_{ch,CH4}} \tag{50}$$

The carbon dioxide emission index can also be determined following Equation [11]:

$$\zeta = \frac{\dot{m}_{CO_2}}{\dot{W}_{net,tot}} \times 3600 \tag{51}$$

4. Results and Discussion

4.1. Validation

4.1.1. Combustion and Chemical Equilibrium Equation

To verify and validate the correctness of the number of moles obtained from combustion products for the main combustor with steam injection, the results from the present analysis were contrasted with the results of reference [21]. Thermodynamic modeling of the CC was performed using the molar balance and the chemical equilibrium conditions of the combustion products, and the molar fractions of the resulting combustion gases are contrasted with the results in reference [21] in Table 3.

Table 3. Comparison of molar fractions of combustion products from the current study with reference [28].

Combustion Product	Molar Fraction Obtained in Current Study with φ = 0.6	Molar Percentage in Reference [28] with φ = 0.6	Molar Fraction Obtained in Current Study with φ = 1.2	Molar Percentage in Reference [28] with φ = 1.2
CO_2	0.05148	0.05151	0.0630	0.0631
H_2O	0.2343	0.2338	0.2789	0.2786
N_2	0.6451	0.6455	0.5944	0.5948
O_2	0.06821	0.06824	4.12×10^{-6}	1.42×10^{-7}
CO	1.76×10^{-6}	3.22×10^{-7}	0.0317	0.0316
H_2	2.9×10^{-6}	5.34×10^{-7}	0.0314	0.0315
H	4.927×10^{-8}	3.84×10^{-9}	2.37×10^{-4}	4.35×10^{-5}
O	1.84×10^{-6}	3.36×10^{-7}	1.08×10^{-6}	3.69×10^{-8}
OH	1.52×10^{-4}	5.46×10^{-5}	2.25×10^{-4}	3.62×10^{-5}
NO	7.70×10^{-4}	8.35×10^{-4}	2.71×10^{-5}	5.39×10^{-6}

Furthermore, for φ = 0.6, the adiabatic temperature for the current study was 1542 K, while for [26], it was 1542.4 K. For φ = 1.2, the adiabatic temperature for the current study was 1971 K, while for [26], it was 1972.6 K.

4.1.2. SCO_2 Subsystem

Table 4 provides a validation of the current results via a comparison with the results of Ref. [24]. The results show the accuracy of the SCO_2 cycle modeling.

Table 4. Validation results obtained in the present work and Ref [24].

State No.	Present Work Temperature (°C)	Ref. [24] Temperature (°C)	Present Work Pressure (kPa)	Ref. [24] Pressure (kPa)	Present Work Mass Flow Rate (kg/s)	Ref. [24] Mass Flow Rate (kg/s)	Present Work Exergy Rate (MW)	Ref. [24] Exergy Rate (MW)
6	550	550	207.2	207.2	2939	2938.18	1557	1556.5
7	428	428.01	74	74	2939	2938.18	1145	1144.5
8	257.6	257.48	74	74	2939	2938.18	851.83	851.29
9	119.5	119.36	74	74	2939	2938.18	690.45	690.05
10	32	32	74	74	2098	2096.18	453.08	452.68
11	97.03	96.88	207.2	207.2	2098	2096.18	520.13	519.55
12	229.9	229.72	207.2	207.2	2939	2938.18	924.24	923.60
13	384.4	384.36	207.2	207.2	2939	2938.18	1200	1199.13

4.2. Power Generation System Case Study

Results are given in Tables 5 and 6 for the GTSC and SIGTSC, respectively, following the power generation system input data of Table 7. Energy and exergy results are provided in Table 8 for both systems.

Table 5. Thermodynamic properties of states of the GTSC power generation system.

State No.	Temperature (K)	Pressure (kPa)	Molar Enthalpy (kJ/kmol)	Molar Entropy (kJ/kmol-K)	Mass Flow Rate (kg/s)	Exergy Rate (kW)
1	298.2	101.3	0	198.6	1	4.473
2	608.7	1013	9246	200.6	1	303.9
3	1300	1013	−2423	228.7	1.023	912.9
4	1026	320.4	−12,138	229.9	1.023	549.1
5	800.6	101.3	−19,755	231.1	1.023	261.1
6	823.2	20,720	23,230	−0.241	0.01503	350.5
7	701.2	7400	17,340	0.701	0.01503	257.8
8	530.8	7400	8789	−13.26	0.01503	191.8
9	392.7	7400	1849	−28.43	0.01503	155.4
10	305.2	7400	−5628	−50.71	0.01073	102
11	370.2	20,720	−4028	−50.06	0.01073	117.1
12	503	20,720	5695	−27.27	0.01503	208.1
13	657.6	20,720	14,246	−12.42	0.01503	270.1
14	686.2	101.3	−23,494	226.1	1.023	180.3
15	298.2	1013	−74,595	167.1	0.02346	1225
16	298.2	101.3	1889	6.61	0.1065	0
17	308.2	101.3	2642	9.096	0.1065	1.316

Table 6. Thermodynamic properties of the states of the SIGTSC power generation system.

State No.	Temperature (K)	Pressure (kPa)	Molar Enthalpy (kJ/kmol)	Molar Entropy (kJ/kmol-K)	Mass Flow Rate (kg/s)	Exergy Rate (kW)
1	298.2	101.3	0	198.6	1	4.473
2	608.7	1013	9246	200.6	1	303.9
3	1300	1013	−16,709	229.7	1.073	1003
4	1029	320.4	−26,443	230.9	1.073	610.1
5	806.4	101.3	−34,104	232.1	1.073	298.2
6	823.2	20,720	23,230	−0.241	0.01706	397.8
7	701.2	7400	17,340	0.701	0.01706	292.5
8	530.8	7400	8789	−13.26	0.01706	217.6
9	392.7	7400	1849	−28.43	0.01706	176.4
10	305.2	7400	−5628	−50.71	0.01218	115.7
11	370.2	20,720	−4028	−50.06	0.01218	132.9
12	503	20,720	5695	−27.27	0.01706	236.1
13	657.6	20,720	14,246	−12.42	0.01706	306.5
14	687.3	101.3	−38,044	226.8	1.073	206.3
15	569.7	101.3	−41,829	220.8	1.073	129.1
16	298.2	101.3	1889	6.61	0.05	26.37
17	298.2	1013	1912	6.606	0.05	26.41
18	573.2	1013	54,951	128.2	0.05	73.03
19	298.2	1013	−74,595	167.1	0.02345	1224
20	298.2	101.3	1889	6.61	0.1208	0
21	308.2	101.3	2642	9.096	0.1208	1.494

Table 7. Input data for modeling the considered power generation system.

T_0 = 298.15 K	Pr_1 = 10	T_{10} = 305.15 K	$\eta_{c,is}$ = 0.87
P_0 = 101.325 kPa	T_{fuel} = 298.15 K	P_{10} = 7400 kPa	η_{cc} = 0.99
T_1 = 298.15 K	T_s = 573.15 K	ε_{LTR} = 0.85	$\eta_{t,is}$ = 0.89
P_1 = 101.325 kPa	s = 5%	PR_c = 2.2–4.2	$\eta_{p,is}$ = 0.70
$\dot{m}_1$ = 1 kg/s	ϕ = 0.4017	$\eta_{t,is,Bottom}$ = 0.9	ε_{HTR} = 0.85
P_{exh} = 101.325 kPa	TIT = 1300 K	$\eta_{is,mc,rc}$ = 0.85	

Table 8. Thermodynamic performance in terms of efficiencies.

Subsystem	Energy Efficiency (%)	Exergy Efficiency (%)
GTSC system		
STIG	25.78	24.95
SCO_2	40.59	67.86
Total	30.41	29.43
SIGTSC system		
SISTIG	30.06	29.09
SCO_2	40.59	67.65
Total	35.31	34.17

Figure 2 depicts a system Sankey diagram, showing the exergy rate of each component flow for the case when the air pressure ratio was equal to 10, the percentage of steam injection was 5%, and the TIT was equal to 1300 K. Also, the pressure ratio in this figure for the SCO_2 subsystem was 2.8. The equivalence ratio was considered to be 0.4017.

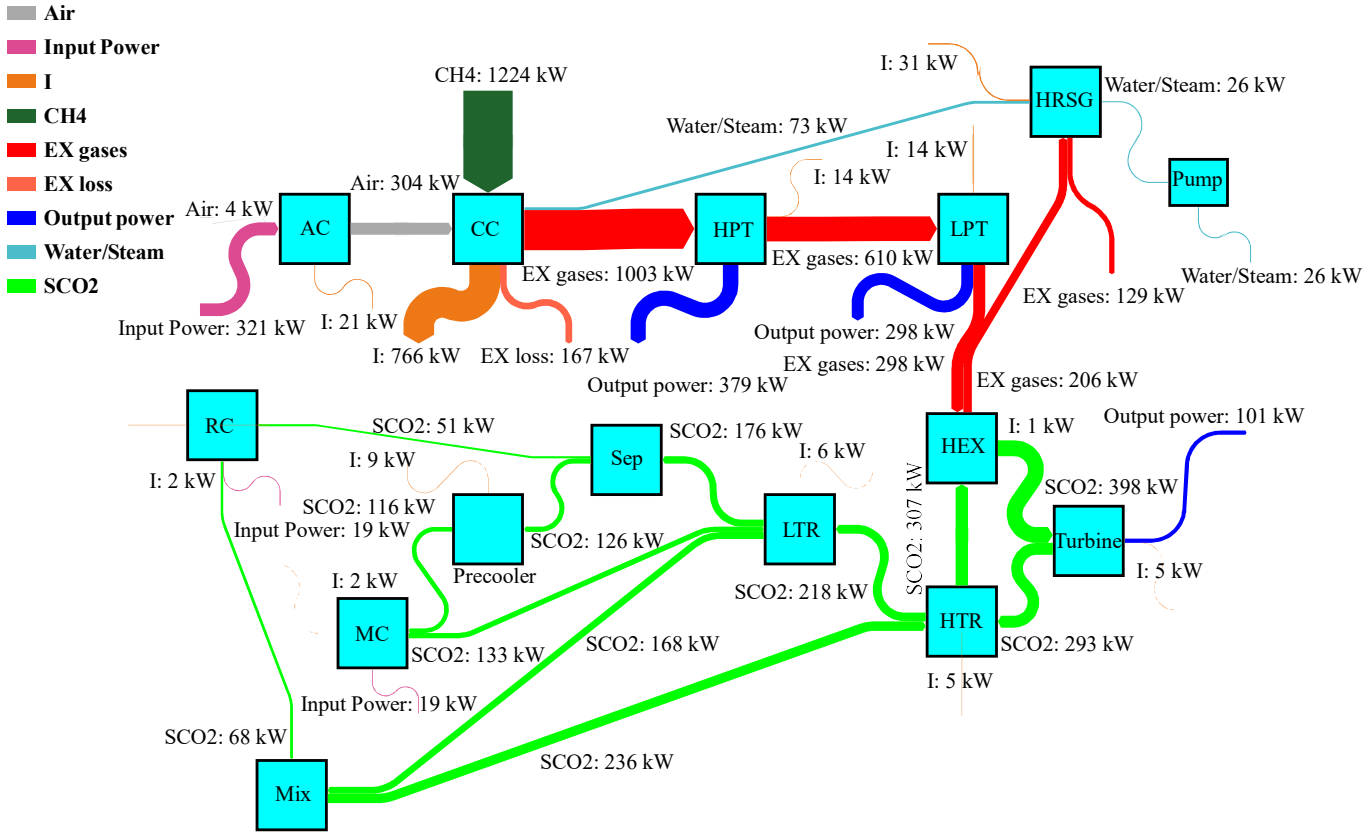

Figure 2. Sankey diagram of SIGTSC.

Figure 3a demonstrates the rates of consumed or generated electric powers of the components of the proposed systems. The negative value of produced power indicates components with power consumption. Component exergy destruction rates are also provided in Figure 3b. According to this figure, the highest and lowest exergy destruction rates were for CC and HEX, respectively (except the pump exhibited the lowest exergy destruction rate for SIGTSC).

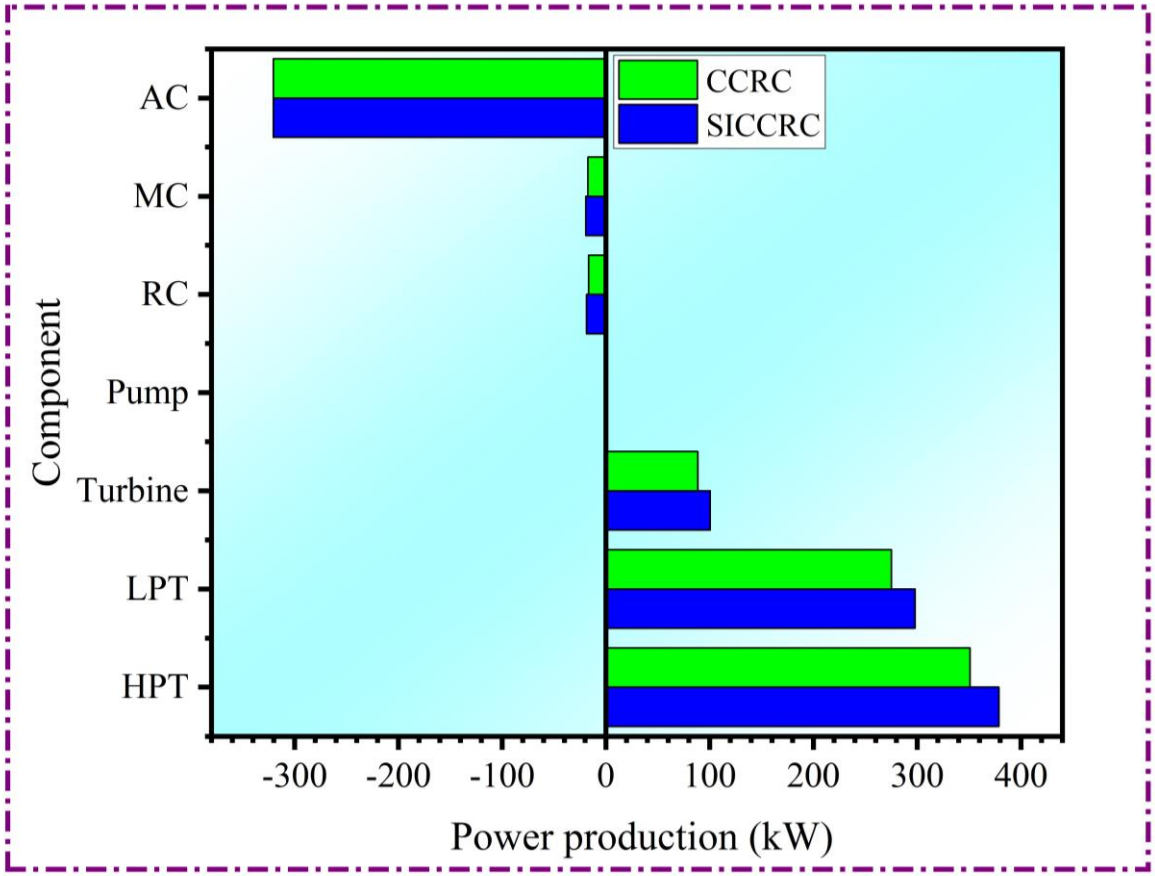

(**a**)

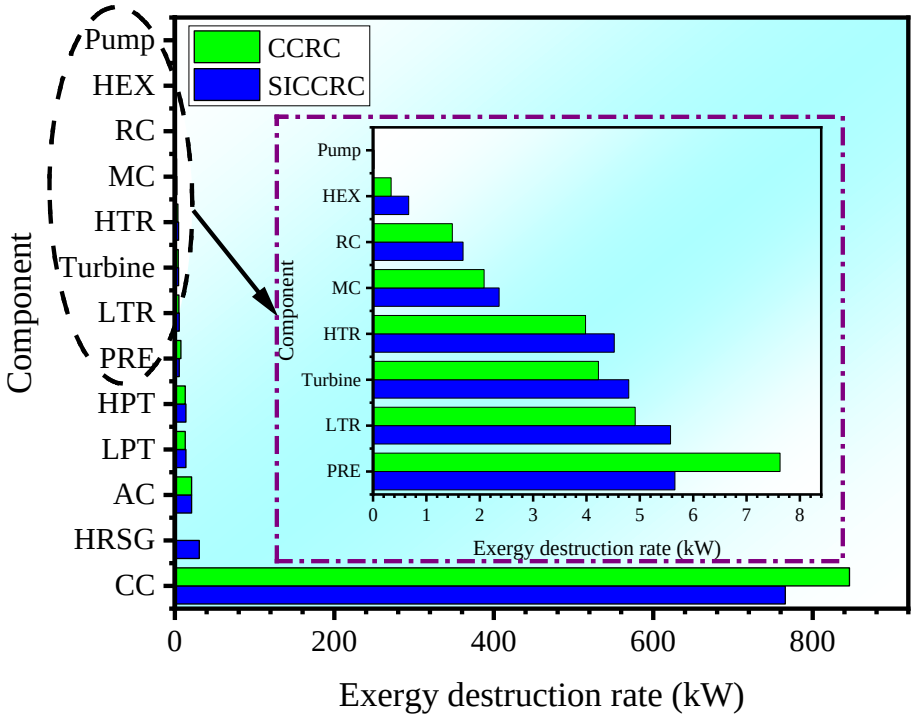

(**b**)

Figure 3. (**a**) Rate of the generated electric power for components of both systems. (**b**) Exergy destruction rates of the components of both systems.

4.3. Parametric Study

Figure 4a illustrates the impact of the equivalence ratio of the CC on the net output power. It is seen that, with rising equivalence ratio, the net output power was augmented. Meanwhile, as steam injection increased from zero to 10%, the net output power rose. Steam injection rose the mass flow rate of the cycle, increasing the net power generation. Raising the equivalence ratio boosted the fuel flow rate. Therefore, the flow rate of the output products also increased; thus, the output work rose. Also, at a specified equivalence ratio, the input flow increased with an increase in the amount of steam injection, and, as a result, the output work increased.

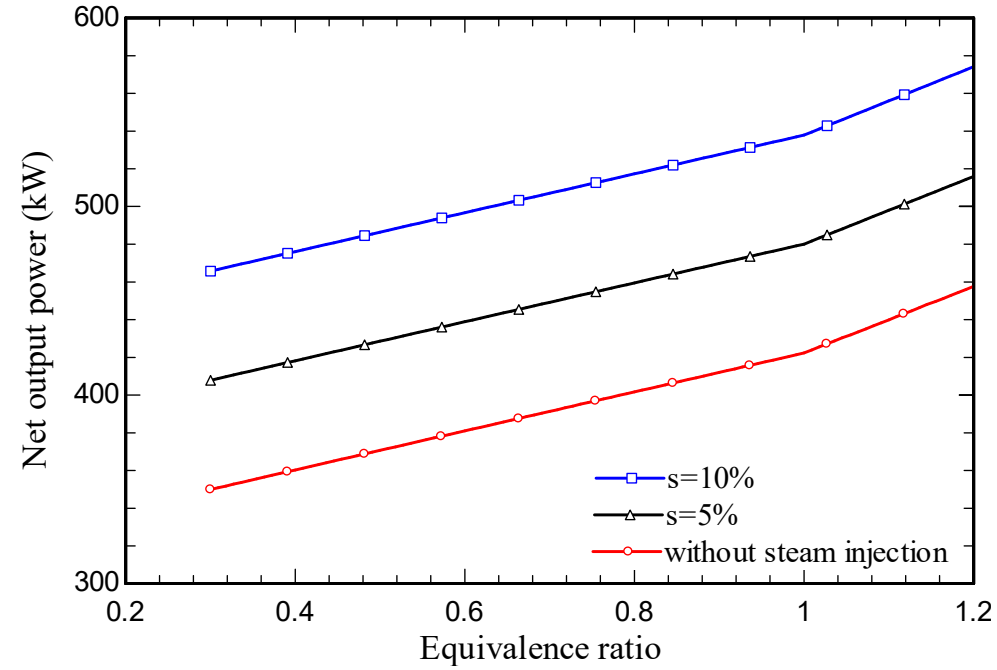

(**a**)

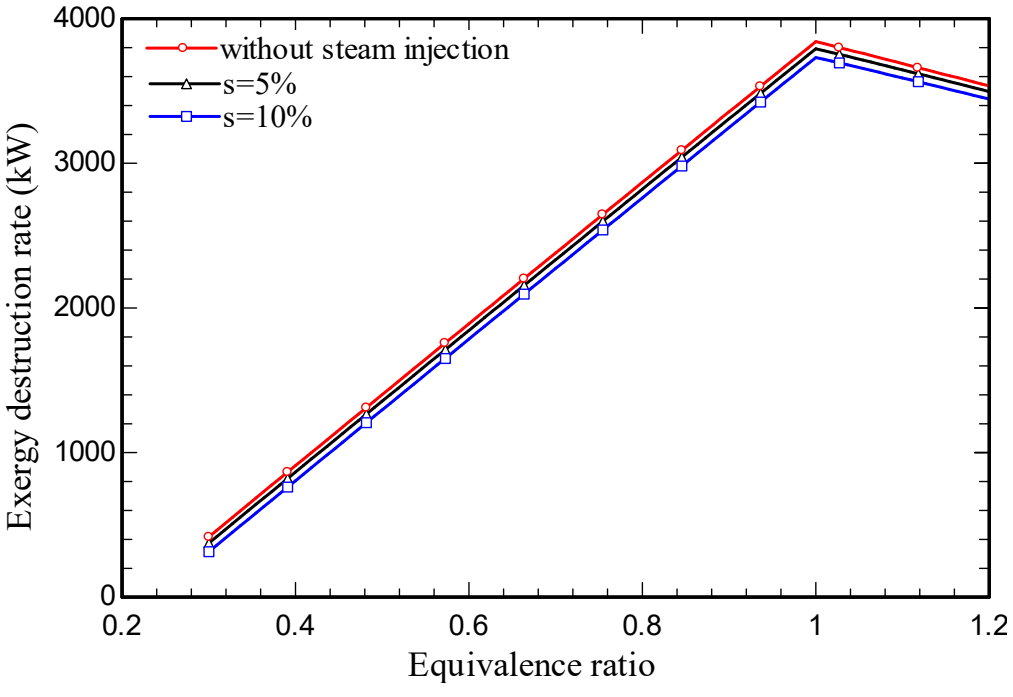

(**b**)

Figure 4. *Cont.*

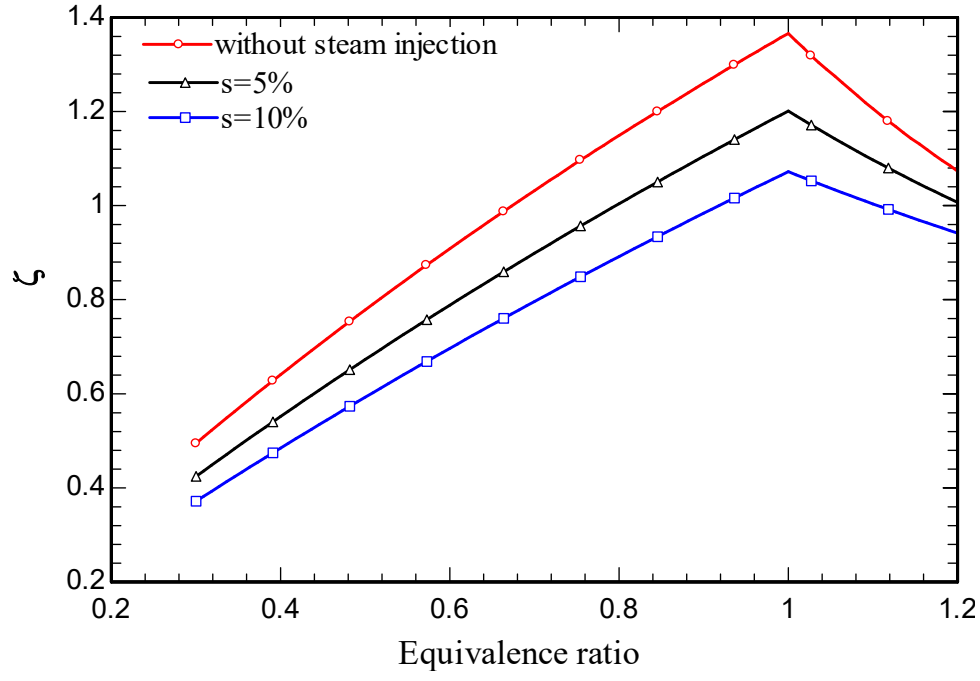

(**c**)

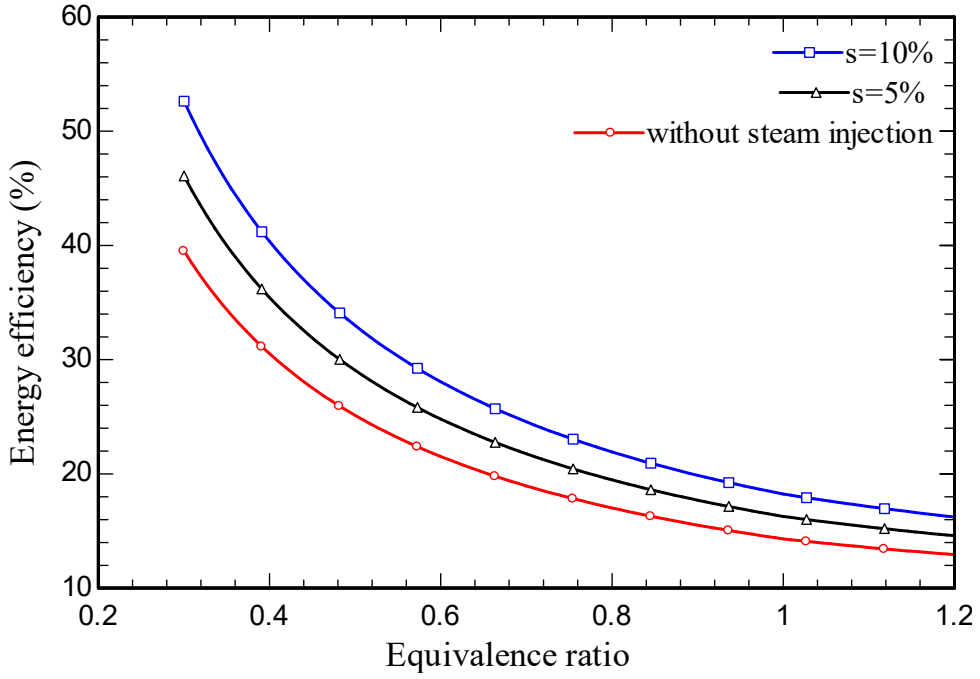

(**d**)

Figure 4. *Cont.*

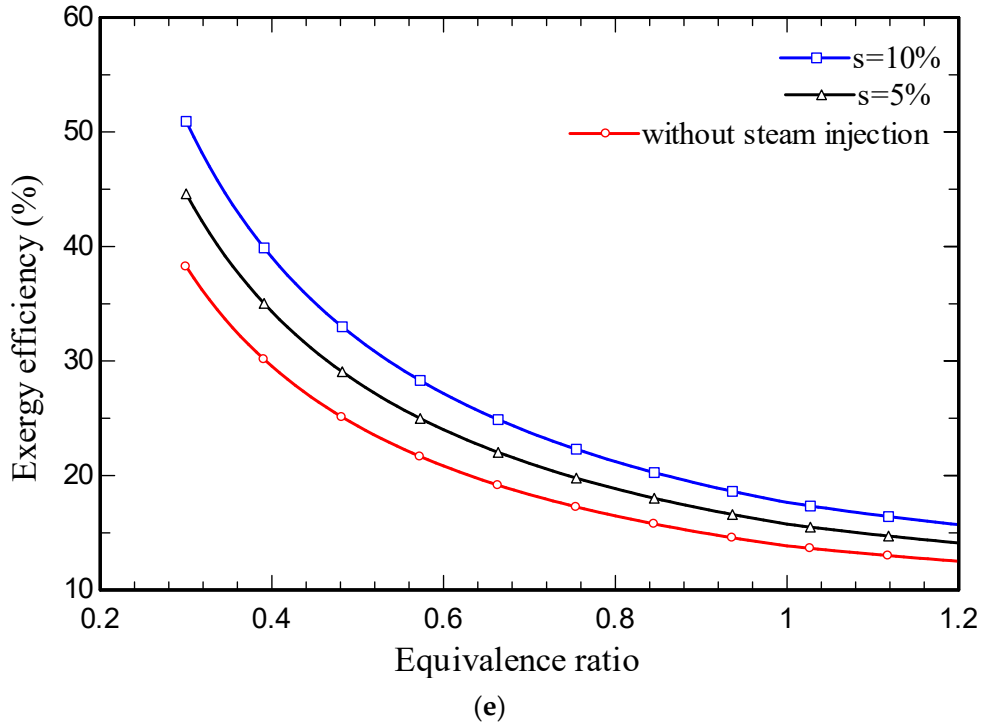

Figure 4. (**a**) Effect on the net output power production of the CC equivalence ratio. (**b**) Effect on the total exergy destruction rate of the equivalence ratio. (**c**) Effect on the CO_2 emission index of the equivalence ratio. (**d**) Effect on the system energy efficiency of the equivalence ratio. (**e**) Effect on the system exergy efficiency of the equivalence ratio.

Figure 4b shows the influence of equivalence ratio on system exergy destruction rate. In this figure, the equivalence ratio rise increased the exergy destruction rate until the stochiometric equivalence ratio decreased. Increasing the quantity of steam injection caused the exergy destruction rate to diminish for a specified equivalence ratio, highlighting the advantage of steam injection in gas cycles.

Figure 4c illustrates the variation with equivalence ratio of CO_2 emission index. With a rise of the equivalence ratio, the mass flow rate of carbon dioxide increased until reaching the stochiometric equivalence ratio and then decreased. According to the increasing trend of carbon dioxide mass flow rate and specific work, the increasing slope of the mass flow rate was higher than the specific work; as a result, the slope of the graph was increasing, but in the rich state, the increasing slope of specific work was higher than the mass flow rate of carbon dioxide, which is shown in Figure 4a, and the general trend was decreasing. According to Figure 4c the value of the CO_2 emission index was reduced as the amount of injected steam into the CC increased.

Figure 4d illustrates the energy efficiency for the overall system as a function of equivalence ratio. An equivalence ratio rise was seen to increase the fuel mass flow rate, lowering the overall energy efficiency. The energy efficiency rose with the steam injection to the CC.

Figure 4e depicts the influence on the exergy efficiency of the overall system equivalence ratio. The trends in exergy and energy efficiency mirrored each other, as described above.

The effects of the variations of turbine inlet temperature (TIT) are shown in Figure 5a–e for five main performance parameters. Figure 5a illustrates the impact of varying TIT on net output power. As the TIT increased, the specific work exhibited an upward trend. This reveals that, with an increase in temperature at the outlet, the enthalpy of the input gases to the turbine also increased and, as a result, the output work increased. Like the trend described above, the more steam that is injected into the CC, the greater net output power derived is.

Impacts on the total exergy destruction rate of the variations of the TIT are illustrated in Figure 5b. Increasing the TIT was seen to decrease the total exergy destruction rate. As the temperature increased, due to approaching the adiabatic flame temperature, the resulting heat loss decreased, so the exergy destruction rate declined. According to Figure 5b, for a constant TIT, the exergy destruction rate diminished with increasing steam injection.

Effects on the carbon dioxide emission index of varying TIT are illustrated in Figure 5c. As shown in the previous section, the exergy destruction rate of the overall system rose with TIT; Figure 5b explains and justifies this behavior.

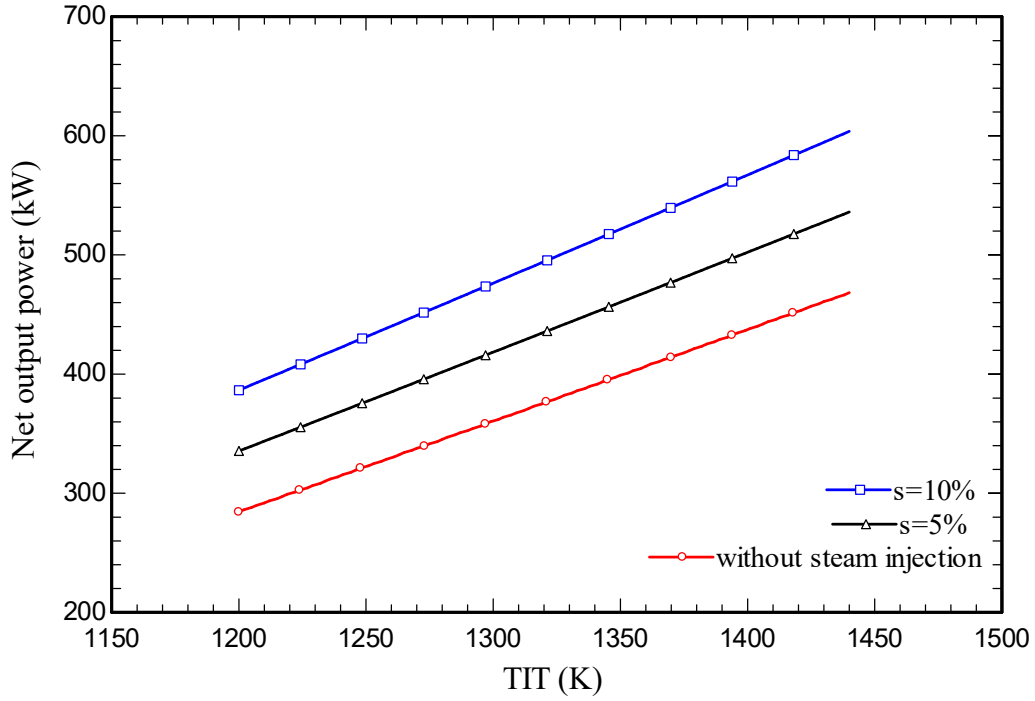

(**a**)

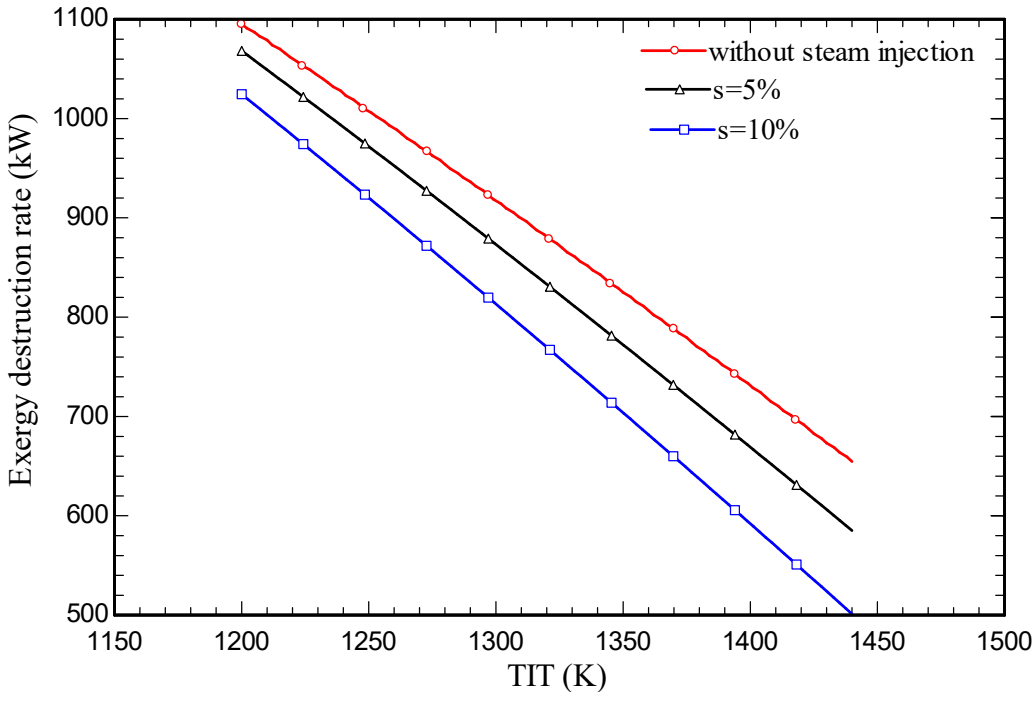

(**b**)

Figure 5. *Cont.*

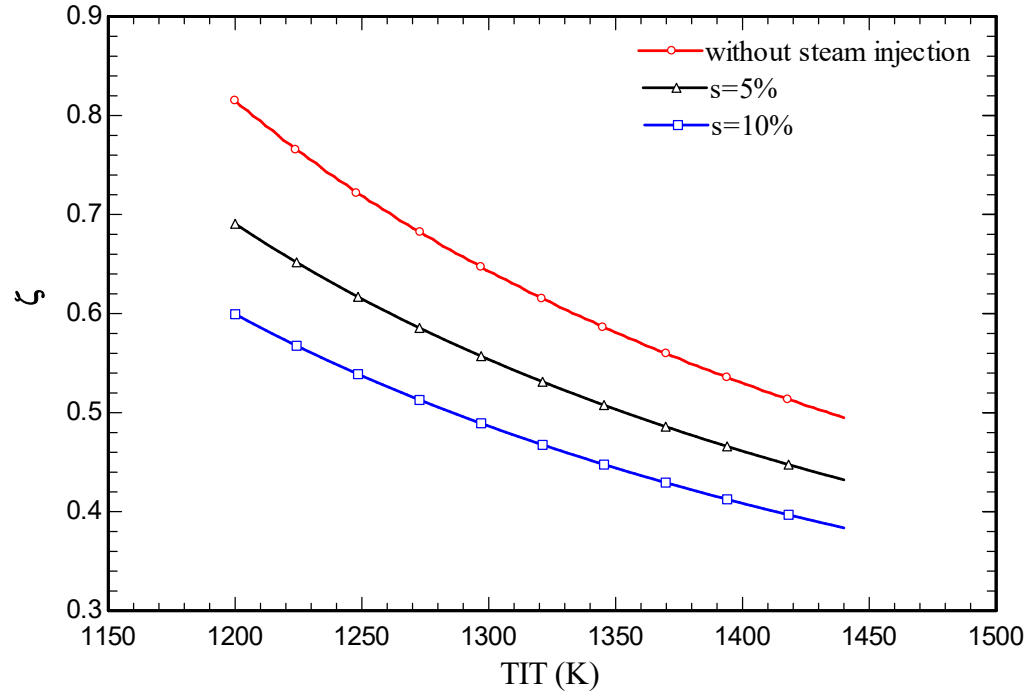

(**c**)

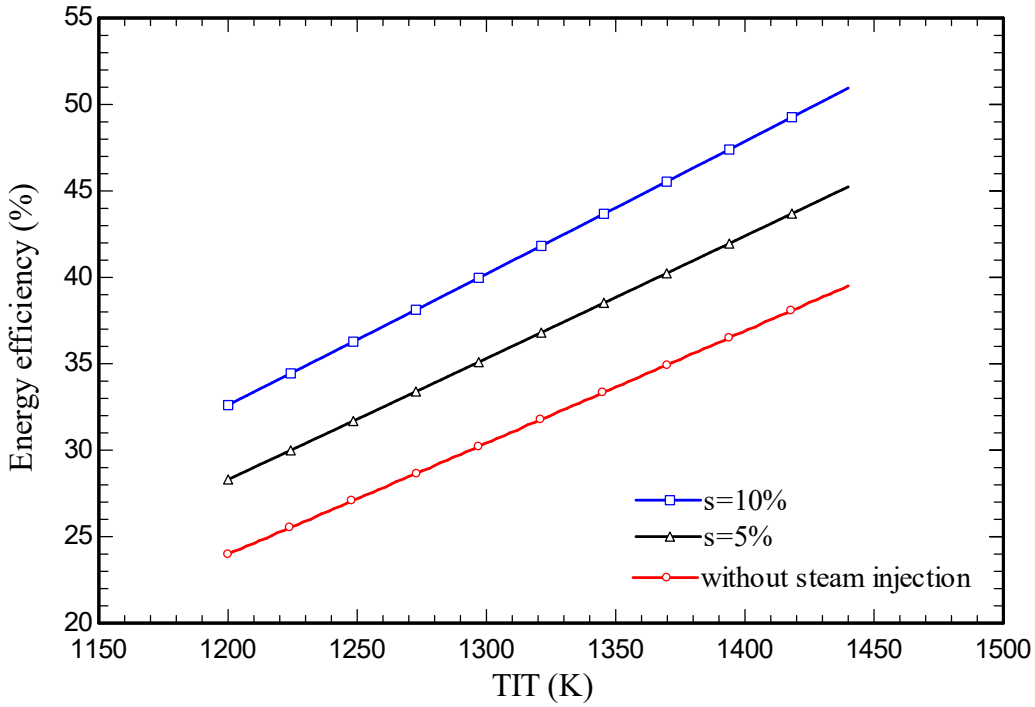

(**d**)

Figure 5. *Cont.*

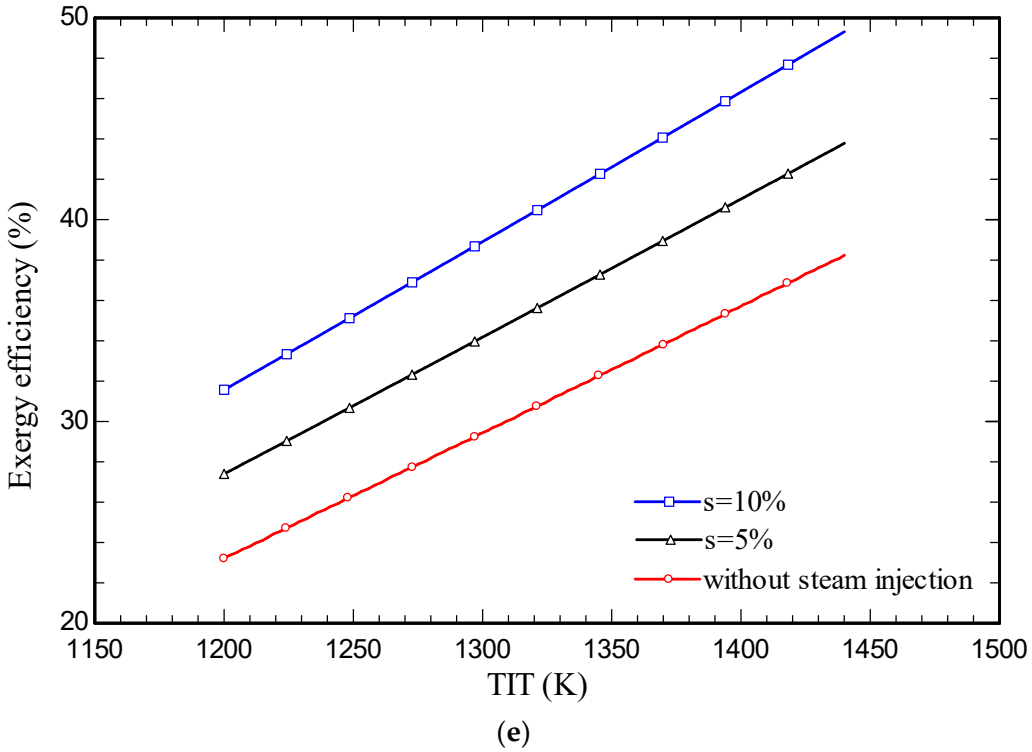

Figure 5. (**a**) Effect on the system net output power of the variation of TIT. (**b**) Effect on the total system exergy destruction rate of the variation of TIT. (**c**) Effect of the variation of TIT on the CO_2 emission index of the system. (**d**) Effect of the variation of TIT on the energy efficiency of the system. (**e**) Effect on the system exergy efficiency of the variation of TIT.

Figure 5d,e show, respectively, the effects on energy and exergy efficiencies of the variations of TIT. As the TIT rose, the energy and exergy efficiencies exhibited similar upward trends, as anticipated.

Figure 6a demonstrates the impact on the system's net power output of varying Pr_1, which attained a maximal value at a specific value of Pr_1 (around 5). As Pr_1 increased, the power produced by the turbines increased. However, as Pr_1 exceeded the optimal value, the system net power decreased because the power used by the compressor exceeded the power generated by the turbines.

Figure 6b presents for the system (including all components), the impact on the total exergy destruction rate of pressure ratio. With climbing pressure ratio, the exergy destruction rate was seen to rise. The system output work increased with pressure ratio, increasing the exergy destruction rate.

The impact of varying pressure ratio on carbon dioxide emission index is seen in Figure 6c. As depicted in Figure 6a, the value of net output power first increased with Pr_1 and then decreased; based on Equation (51), the trend of carbon dioxide emission index was inverse to the net output power.

Figure 6d,e show the respective impacts on system energy and exergy efficiencies of variations of Pr_1. Meanwhile, the energy and exergy efficiencies were observed to increase and then to decrease while decreasing the net output power (Equations (41) and (49)). Note that there was a straight relation between both energy and exergy efficiencies and net output power. Both efficiency trends were similar and had maximum points.

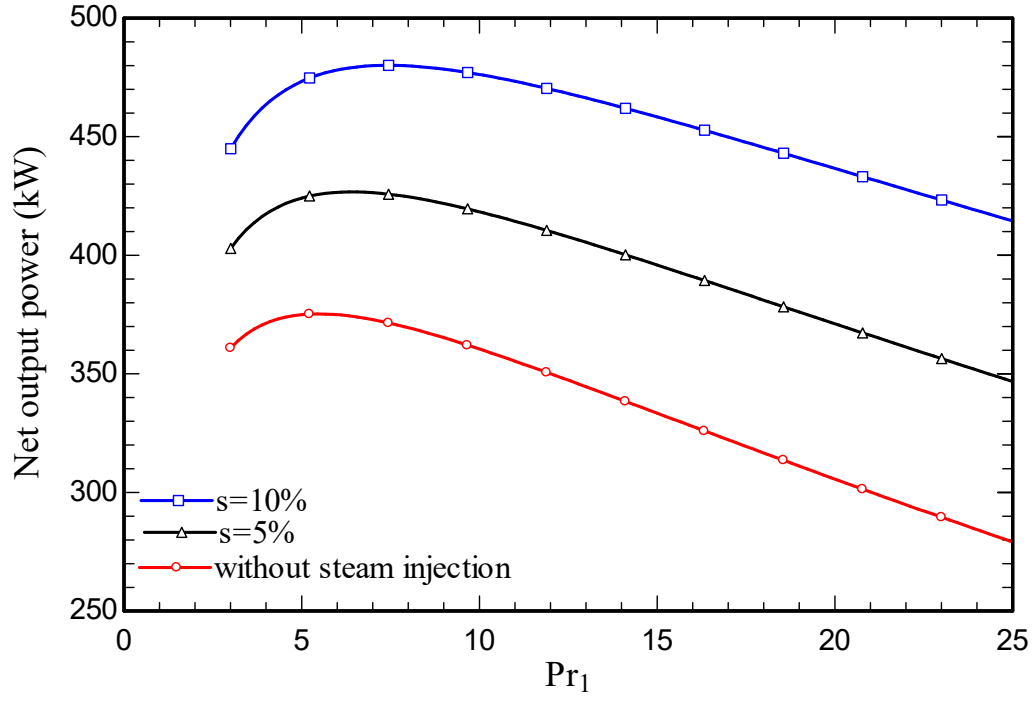

(**a**)

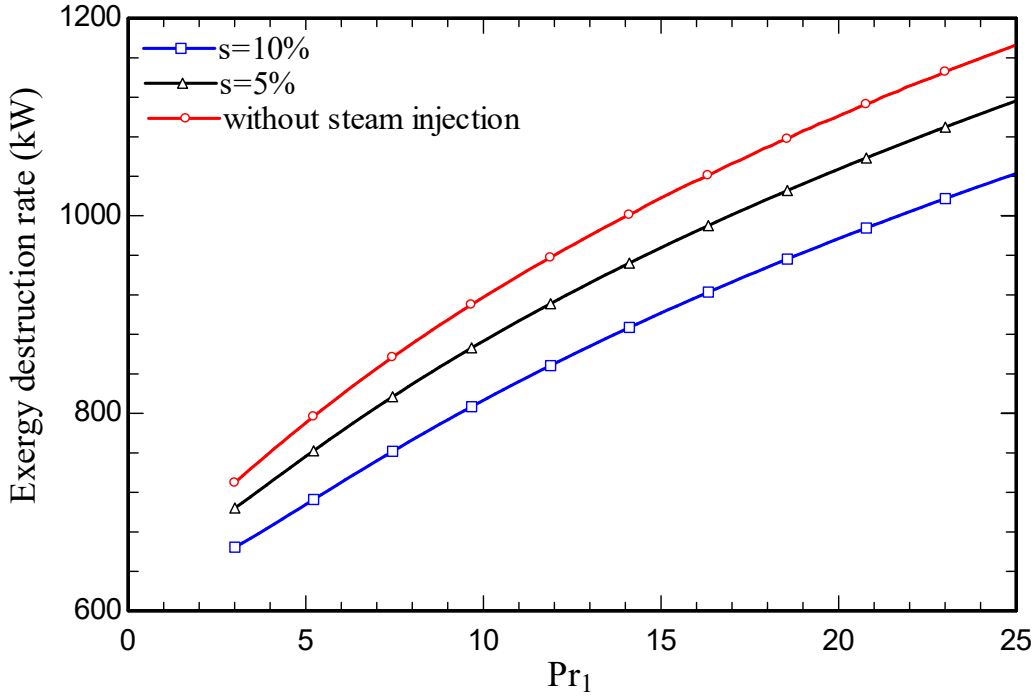

(**b**)

Figure 6. *Cont.*

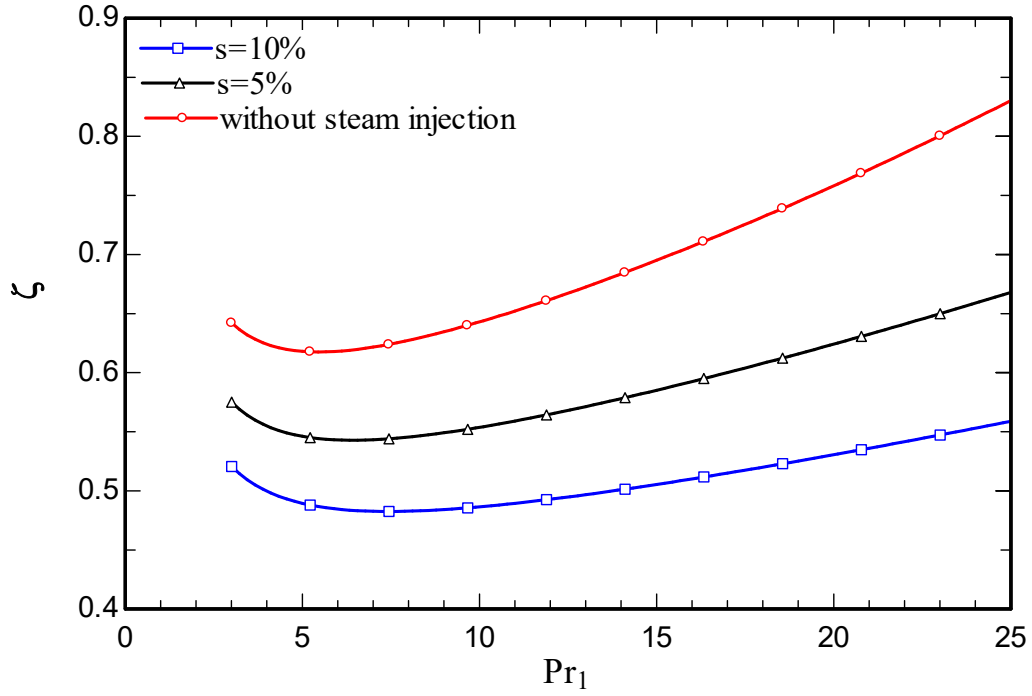

(**c**)

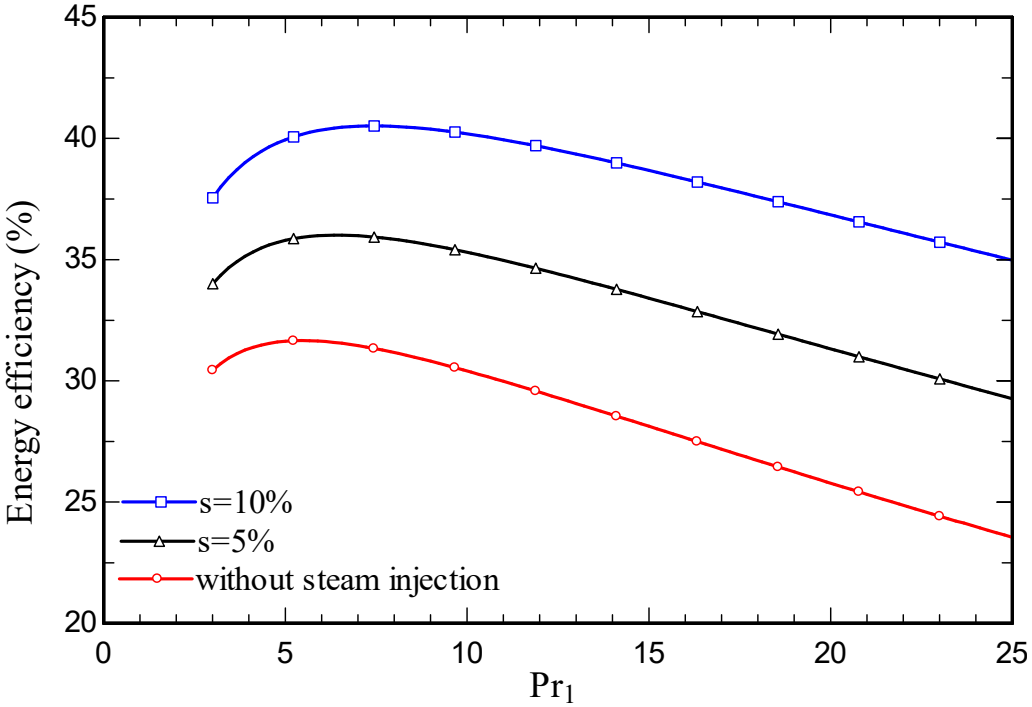

(**d**)

Figure 6. *Cont.*

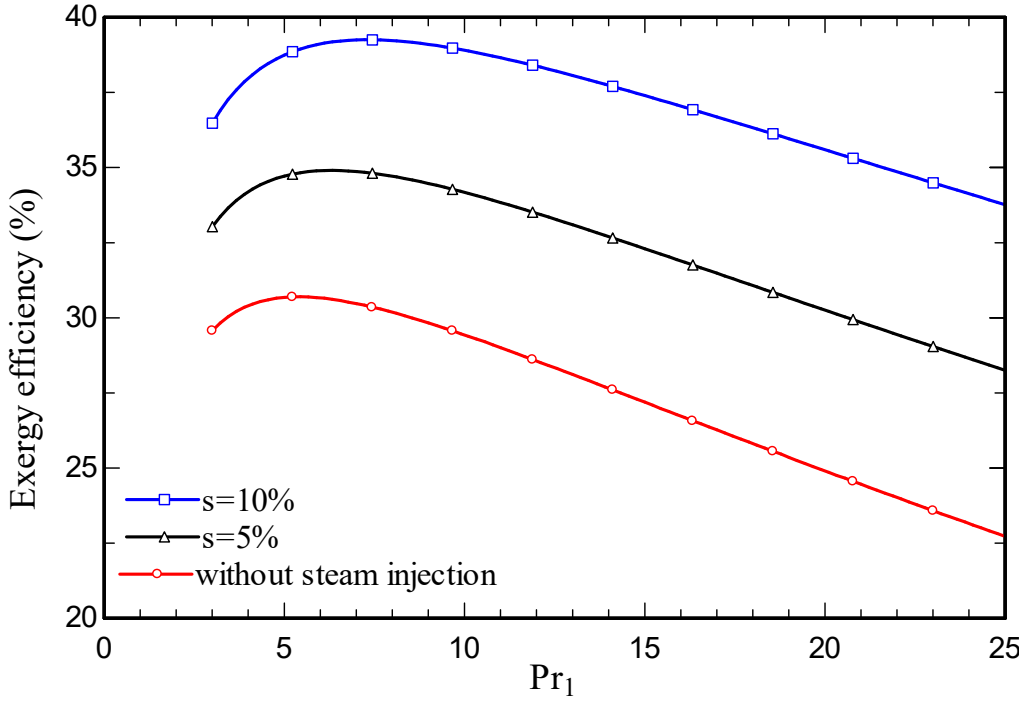

Figure 6. (**a**) Effect on the system net power output of variation of Pr_1. (**b**) Effect on the system total exergy destruction rate of the variation of Pr_1. (**c**) Effect of the variation of Pr_1 on CO_2 emission index of the system. (**d**) Effect of the variation of Pr_1 on the energy efficiency of the system. (**e**) Effect of the variation of Pr_1 on the exergy efficiency of the system.

Figure 7 portrays how the system's bottom cycle pressure ratio affected the net output power. As the bottom cycle's pressure ratio rose, the net output power intensified. The subsystem pressure ratio had a small impact on the main parameters in both cases examined, so further attention was not placed on the phenomenon. As the quantity of injected steam rose, the net output power improved.

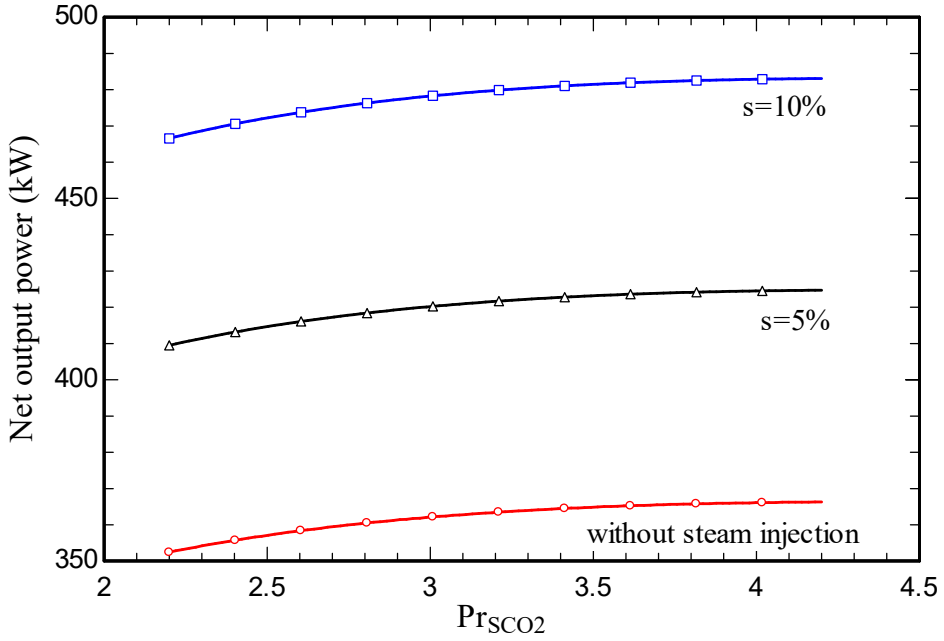

Figure 7. Effect of variation on the system net output power of the bottom cycle pressure ratio.

5. Conclusions

A combined cycle comprised of a gas turbine with two stages and steam injection coupled with a SCO_2 subsystem cycle was investigated, considering energy and exergy aspects. Furthermore, in the case study and parametric study, the behaviors of both GTSC and SIGTSC systems were assessed separately. For both cycles, the combustion chamber was examined in-depth so that the modeling was more realistic.

The main findings of the research and the conclusions drawn from them are as follows:

- Increasing the amount of steam injection improved the system net output power and lowered the exergy destruction rate. Moreover, it reduced the carbon dioxide emission index.
- Steam injection in the SIGTSC reduced the heat loss of the combustion chamber compared to the GTSC.
- Energy and exergy efficiencies of 35.3% and 34.1%, respective, were obtained for the SIGTSC, which were greater than the corresponding values for the GTSC: 30.4% and 29.4%. Steam injection improved the thermodynamic efficiency.
- Due to the combustion chamber's design temperature limitations for this configuration, TIT could only vary within a certain range. In addition, at 1440 K, the CC was considered almost adiabatic.

Author Contributions: Conceptualization, S.H.F.A., A.J., S.M.S.M., S.S. and M.A.R.; Methodology, S.H.F.A., A.J., S.M.S.M., S.S. and M.A.R.; Software, S.H.F.A., A.J., S.M.S.M., S.S. and M.A.R.; Validation, S.H.F.A., A.J. and S.M.S.M.; Formal analysis, S.H.F.A., A.J., S.M.S.M., S.S. and M.A.R.; Investigation, S.H.F.A., A.J., S.M.S.M., S.S. and M.A.R.; Resources, S.H.F.A., A.J., S.M.S.M., S.S. and M.A.R.; Data curation, S.H.F.A., A.J., S.M.S.M., S.S. and M.A.R.; Writing—original draft, S.H.F.A., A.J., S.M.S.M., S.S. and M.A.R.; writing—review and editing, S.H.F.A., A.J., S.M.S.M., S.S. and M.A.R.; visualization, S.H.F.A., A.J., S.M.S.M., S.S. and M.A.R.; supervision, S.M.S.M., S.S. and M.A.R. All authors have read and agreed to the published version of the manuscript.

Funding: This research received no external funding.

Institutional Review Board Statement: Not applicable.

Informed Consent Statement: Not applicable.

Data Availability Statement: Not applicable.

Conflicts of Interest: The authors declare no conflict of interest.

Nomenclature

CC	Combustion chamber
$\dot{E}_{ch}$	Chemical flow exergy rate (kW)
$\dot{E}_e$	Outlet exergy flow rate (kW)
$\dot{E}_i$	Inlet exergy flow rate (kW)
$\overline{e}_i^{ch.0}$	Standard chemical exergy of an ideal gas
$\dot{E}_{th}$	Thermodynamic flow exergy (kW)
GTSC	Gas turbine with supercritical carbon dioxide
$\overline{g}_i$	Molar Gibbs function (kJ/kmol)
$\dot{H}$	Enthalpy rate (kW)
HEX	Heat exchange
HRSG	Heat recovery steam generator
HTR	High temperature recuperator
$\dot{I}_{cv}$	Internal irreversibility rate (kW)
K_s	Equilibrium constant
LHV	Lower heating value
LTR	Low temperature recuperator

$\dot{m}_1$	Air mass flow rate (kg/s)
P_0	Ambient pressure (kPa)
P_1	Compressor inlet pressure (kPa)
P_{10}	State 10 pressure (kPa)
P_{exh}	Exhaust pressure (kPa)
Pr_1	Air compressor pressure ratio
PR_c	Bottom cycle pressure ratio
$\dot{Q}_{cv}$	Heat transfer rate (kW)
s	Steam injection ratio (%)
SCO_2	Supercritical carbon dioxide
SIGTSC	Steam injection gas turbine with supercritical carbon dioxide
STIG	Steam injection gas turbine
T_0	Ambient temperature (K)
T_1	Air compressor inlet temperature (K)
T_{10}	State 10 temperature (K)
T_{fuel}	Fuel temperature (K)
$T_{product}$	Product temperature (K)
T_s	Steam temperature (K)
TIT	Turbine inlet temperature (K)
$\dot{W}_{cv}$	Production or consumption power (kW)
WSR	Well-stirred reactor
x	Molar injection ratio of H_2O to air
y_i	Molar fraction of species i in a mixture
ε	Molar air-fuel ratio
ϕ	Equivalence ratio
ν	Number of moles of combustion products
ε_{HTR}	Heat exchange efficiency for HTR (%)
ε_{LTR}	Heat exchange efficiency for LTR (%)
$\eta_{c,is}$	Air compressor isentropic efficiency (%)
η_{cc}	Combustion chamber efficiency (%)
$\eta_{t,is}$	Turbine isentropic efficiency (%)
$\eta_{p,is}$	Pump isentropic efficiency (%)
$\eta_{t,is,Bottom}$	Bottom cycle turbine isentropic efficiency (%)
$\eta_{is,mc,rc}$	Bottom cycle compressor isentropic efficiency (%)
η_I	Energy efficiency (%)
η_{II}	Exergy efficiency (%)
ζ	Carbon dioxide emission index

References

1. Fetisov, V.; Gonopolsky, A.M.; Davardoost, H.; Ghanbari, A.R.; Mohammadi, A.H. Regulation and impact of VOC and CO_2 emissions on low-carbon energy systems resilient to climate change: A case study on an environmental issue in the oil and gas industry. *Energy Sci. Eng.* **2023**, *11*, 1516–1535. [CrossRef]
2. Fetisov, V.; Gonopolsky, A.M.; Zemenkova, M.Y.; Andrey, S.; Davardoost, H.; Mohammadi, A.H.; Riazi, M. On the Integration of CO_2 Capture Technologies for an Oil Refinery. *Energies* **2023**, *16*, 865. [CrossRef]
3. Competitiveness of US Gas Turbine Manufacturers. Available online: https://gasturbine.org/docs/newdocs/YAGTP4602_GTA%20White%20Paper_041013%20final.pdf (accessed on 17 September 2023).
4. Jansohn, P. *Modern Gas Turbine Systems: High Efficiency, Low Emission, Fuel Flexible Power Generation*; Woodhead Publishing Series in Energy; Elsevier Science: Amsterdam, The Netherlands, 2013; ISBN 9781845697280.
5. Kayadelen, H.; Ust, Y. Performance and environment as objectives in multi-criterion optimization of steam injected gas turbine cycles. *Appl. Therm. Eng.* **2014**, *71*, 184–196. [CrossRef]
6. Lu, M.; Li, D.; Xie, K.; Sun, G.; Fu, Z. Investigation of flame evolution and stability characteristics of H_2-enriched natural gas fuel in an industrial gas turbine combustor. *Fuel* **2023**, *331*, 125938. [CrossRef]
7. Ren, J.; Qian, Z.; Fei, C.; Lu, D.; Zou, Y.; Xu, C.; Liu, L. Thermodynamic, exergoeconomic, and exergoenvironmental analysis of a combined cooling and power system for natural gas-biomass dual fuel gas turbine waste heat recovery. *Energy* **2023**, *269*, 126676. [CrossRef]
8. Kayadelen, H.; Ust, Y. Thermoenvironomic evaluation of simple, intercooled, STIG, and ISTIG cycles. *Int. J. Energy Res.* **2018**, *42*, 3780–3802. [CrossRef]

9. Kayadelen, H.; Ust, Y.; Başhan, V. Thermodynamic performance analysis of state of the art gas turbine cycles with inter-stage turbine reheat and steam injection. *Energy* **2021**, *222*, 119981. [CrossRef]
10. YERANEE, K.; RAO, Y. A review of recent studies on rotating internal cooling for gas turbine blades. *Chin. J. Aeronaut.* **2021**, *34*, 85–113. [CrossRef]
11. Javaherian, A.; Yari, M.; Gholamian, E.; Carton, J.G.; Mehr, A.S. Proposal and comprehensive analysis of power and green hydrogen production using a novel integration of flame-assisted fuel cell system and Vanadium-Chlorine cycle: An application of multi-objective optimization. *Energy Convers. Manag.* **2023**, *277*, 116659. [CrossRef]
12. Sinha, A.A.; Saini, G.; Sanjay; Shukla, A.K.; Ansari, M.Z.; Dwivedi, G.; Choudhary, T. A novel comparison of energy-exergy, and sustainability analysis for biomass-fueled solid oxide fuel cell integrated gas turbine hybrid configuration. *Energy Convers. Manag.* **2023**, *283*, 116923. [CrossRef]
13. Ryu, B.; Duong, P.A.; Kang, H. Comparative analysis of the thermodynamic performances of solid oxide fuel cell–gas turbine integrated systems for marine vessels using ammonia and hydrogen as fuels. *Int. J. Nav. Archit. Ocean Eng.* **2023**, *15*, 100524. [CrossRef]
14. Bolland, O.; Stadaas, J. Comparative Evaluation of Combined Cycles and Gas Turbine Systems With Water Injection, Steam Injection, and Recuperation. *J. Eng. Gas Turbines Power-Trans. ASME* **1995**, *117*, 138–145. [CrossRef]
15. Jonsson, M.; Yan, J. Humidified gas turbines–A review of proposed and implemented cycles. *Energy* **2005**, *30*, 1013–1078. [CrossRef]
16. Roumeliotis, I.; Mathioudakis, K. Evaluation of water injection effect on compressor and engine performance and operability. *Appl. Energy* **2010**, *87*, 1207–1216. [CrossRef]
17. Eshati, S.; Abu, A.; Laskaridis, P.; Khan, F. Influence of water–air ratio on the heat transfer and creep life of a high pressure gas turbine blade. *Appl. Therm. Eng.* **2013**, *60*, 335–347. [CrossRef]
18. Renzi, M.; Riolfi, C.; Baratieri, M. Influence of the Syngas Feed on the Combustion Process and Performance of a Micro Gas Turbine with Steam Injection. *Energy Procedia* **2017**, *105*, 1665–1670. [CrossRef]
19. Mazzucco, A.; Rokni, M. Thermo-economic analysis of a solid oxide fuel cell and steam injected gas turbine plant integrated with woodchips gasification. *Energy* **2014**, *76*, 114–129. [CrossRef]
20. Amiri Rad, E.; Kazemiani, P. Thermo-environmental and economic analyses of an integrated heat recovery steam-injected gas turbine. *Energy* **2017**, *141*, 1940–1954. [CrossRef]
21. Salem Ahmed, M.; Mohamed Aly, H. Performance characteristics of modified gas turbine cycles with steam injection after combustion exit. *Int. J. Energy Res.* **2012**, *36*, 1346–1357. [CrossRef]
22. Bahrami, S.; Ghaffari, A.; Thern, M. Improving the Transient Performance of the Gas Turbine by Steam Injection during Frequency Dips. *Energies* **2013**, *6*, 5283–5296. [CrossRef]
23. Lei, S.; Wang, D.; Xie, Y. Energy, Exergy and exergoeconomic analysis of two supercritical CO_2 cycles for waste heat recovery of gas turbine. *Appl. Therm. Eng.* **2021**, *196*, 117337. [CrossRef]
24. Wu, C.; Wang, S.; Feng, X.; Li, J. Energy, exergy and exergoeconomic analyses of a combined supercritical CO_2 recompression Brayton/absorption refrigeration cycle. *Energy Convers. Manag.* **2017**, *148*, 360–377. [CrossRef]
25. Akbari, A.D.; Mahmoudi, S.M.S. Thermoeconomic analysis & optimization of the combined supercritical CO_2 (carbon dioxide) recompression Brayton/organic Rankine cycle. *Energy* **2014**, *78*, 501–512. [CrossRef]
26. Lefebvre, A.H.; Ballal, D.R. *Gas Turbine Combustion: Alternative Fuels and Emissions*, 3rd ed.; CRC Press: Boca Raton, FL, USA, 2010; ISBN 9781420086058.
27. Kim, Y.; Kim, C.G.; Favrat, D. Transcritical or supercritical CO_2 cycle using both low-and high-temperature heat sources. *Energy* **2012**, *43*, 402–415. [CrossRef]
28. Kayadelen, H.K.; Ust, Y. Prediction of equilibrium products and thermodynamic properties in H_2O injected combustion for $C_\alpha H_\beta O_\gamma N_\delta$ type fuels. *Fuel* **2013**, *113*, 389–401. [CrossRef]
29. Kayadelen, H.K. A multi-featured model for estimation of thermodynamic properties, adiabatic flame temperature and equilibrium combustion products of fuels, fuel blends, surrogates and fuel additives. *Energy* **2018**, *143*, 241–256. [CrossRef]
30. Poullikkas, A. An overview of current and future sustainable gas turbine technologies. *Renew. Sustain. Energy Rev.* **2005**, *9*, 409–443. [CrossRef]
31. Moran, M.J.; Shapiro, H.N.; Boettner, D.D.; Bailey, M.B. *Fundamentals of Engineering Thermodynamics*; Wiley: Hoboken, NJ, USA, 2010; ISBN 9780470495902.
32. Bejan, A.; Tsatsaronis, G.; Moran, M.J. *Thermal Design and Optimization*; Wiley: Hoboken, NJ, USA, 1995; ISBN 9780471584674.
33. Wark, K. *Advanced Thermodynamics for Engineers*; McGraw-Hill: New York, NY, USA, 1995; ISBN 9780070682924.

Disclaimer/Publisher's Note: The statements, opinions and data contained in all publications are solely those of the individual author(s) and contributor(s) and not of MDPI and/or the editor(s). MDPI and/or the editor(s) disclaim responsibility for any injury to people or property resulting from any ideas, methods, instructions or products referred to in the content.